Construction and Building Materials 341 (2022) 127777

Contents lists available at ScienceDirect

Construction and Building Materials

journal homepage: www.elsevier.com/locate/conbuildmat

Assessment of the ability of MGO based binary binders for the substitution of Portland cement for mortars manufacturing

A. Seco [a,*], J.M. del Castillo [a], S. Espuelas [a], S. Marcelino [b], A.M. Echeverría [c]

[a] Institute of Smart Cities, Public University of Navarre, 31006 Pamplona, Spain
[b] Dept. of Engineering, Public University of Navarre, 31006 Pamplona, Spain
[c] Zabala Innovation Consulting S.A, 31192 Mutilva, Spain

ARTICLE INFO

Keywords:
MgO
GGBS
Magnesium silicate hydrate (M-S-H)
Binary binder
Mortar

ABSTRACT

This article evaluates the ability of a magnesia kiln dust (PC-8) and a commercial calcined MgO (MCB100), combined with ground granulated blastfurnace slag (GGBS), as constituents of binary M-S-H binders. Mortars and pastes were manufactured and their properties were compared to those of Portland Cement (PC). MgO-based mortars showed an increase in setting time and higher fresh consistency. At earlier ages MgO mortars showed lower mechanical properties. At 90 days both MgO-based mortars overcame the PC flexural strength and PC-8 + GGBS also overcame its compressive strength. X-Ray Diffraction and Thermogravimetry tests demonstrated the presence of M-S-H in the pastes.

1. Introduction

MgO-based hydraulic binders are receiving increasing interest because of their potential as alternative to Portland Cement (PC). Reactive MgO in MgO-SiO_2-H_2O systems form poorly ordered nanosized phyllosilicates with cementitious properties known as magnesium silicate hydrates (M-S-H) [1-3]. Nowadays most of MgO is obtained by calcination of natural magnesite rocks ($MgCO_3$) that, by firing, decarbonize as shown in Eq. (1), releasing about 1.1–1.4 kg of CO_2 for the production of 1 kg of MgO [4-6].

$$MgCO_3 \rightarrow MgO + CO_2 \quad (1)$$

The most important parameter of the magnesite rocks calcination is the calcining temperature as it determines the properties of the MgO manufactured. Below 1,000 °C MgO crystals have lower size, high porosity and high specific surface area (SSA). As a result, MgO shows a high level of reactivity. Increasing the calcination temperature at > 1,000 °C, MgO crystals' size increases and SSA and reactivity reduces [4,7-9]. Magnesite is a scarce and expensive raw material that is mainly consumed for the manufacturing of refractory materials for the industry [10]. Commercial magnesite calcination is carried out in rotary kilns with crosscurrent air as shown in Fig. 1.

Magnesite rocks enter in the combustion chamber and advance as the kiln rotates. As magnesite advances it is heated and thereby decarbonized by the combustion gases and the direct flame of the fuel burning. After burning calcined magnesite is air cooled before leaving the kiln. During the calcination, the countercurrent flow pulls dust magnesite particles along the combustion chamber that are collected in cyclones before the venting of gases to the atmosphere. This magnesia kiln dust (MKD) contains a mix of unburned magnesite, calcined MgO and eventually sintered MgO, depending on the part of the combustion chamber where they were pulled from and the higher temperature they were exposed to. The amount of MKD production supposes about 30% of the calcined magnesite manufactured and it is usually marketed as a low grade MgO byproduct. Published works have demonstrated the MKD ability as a binder constituent for clay, expansive and sulfate soils stabilization [11-13] and for the unfired clay bricks manufacturing [14,15]. Nonetheless, nowadays the total consumption of MKD is lower than its production, being an increasing economic and environmental concern for the MgO industry, due to the world growing needs of refractory materials [16]. Thus, new applications for this low grade reactive MgO are required. The aim of this study has been to evaluate the ability of a MKD and a commercial reactive MgO, combined with ground granulated blastfurnace slag (GGBS), as constituents of binary M-S-H binder systems for the production of ordinary masonry mortars. For this, an experimental laboratory investigation of MKD-GGBS and MgO +

* Corresponding author.
E-mail addresses: andres.seco@unavarra.es (A. Seco), jesusmaria.delcastillo@unavarra.es (J.M. del Castillo), sandra.espuelas@unavarra.es (S. Espuelas), sara.marcelino@unavarra.es (S. Marcelino), amecheverria@zabala.es (A.M. Echeverría).

https://doi.org/10.1016/j.conbuildmat.2022.127777
Received 31 January 2020; Received in revised form 3 May 2022; Accepted 5 May 2022
Available online 20 May 2022

GGBS mortars and pastes was carried out. PC was considered as reference. Fresh consistency, setting time, density, flexural strength and compressive strength tests were conducted to characterize the magnesium-based mortars fresh and cured properties as construction materials. pH, X Ray Diffraction (XRD) and thermogravimetric analysis were carried out to state the M-S-H gels formation.

2. Materials and methods

2.1. Materials

Two MgO sources were used in the laboratory investigation: A high reactive commercial MgO obtained from magnesite rocks calcined at 1,100 °C, marketed as MCB100. The second MgO material was a MKD recovered from the combustion gases of two kilns, working at 1,100 °C and 1,800 °C respectively. This co-product is marketed under the name PC-8. Both MgO samples were supplied by *Magnesitas Navarras S.A.* company that produce them in its factory located in Zubiri (Spain). Table 1 shows the chemical composition, parameters representative of the reactivity and Fig. 2 shows the granulometry of the constituents of the binders considered for the laboratory investigation.

GGBS is a by-product obtained during the manufacturing of pig iron. It is formed by rapid cooling of molten iron slag to maintain an amorphous structure and it is grinded in order to increase its reactivity. The sample available for this investigation was provided by Heidelberg Cement Group (UK). As shown in Table 1, it has a big cementitious potential because of its richness in reactive calcium, silicon and aluminum oxides. PC used in this study was manufactured in accordance with the European Standard EN 197–1 and is marketed in Spain under the trade name CEM II/B-L 32.5 N. As aggregate for the mortars manufacturing a commercial calcareous 0–4 mm sand from limestone crushing was used.

2.2. Samples preparation

Pastes and mortars were manufactured for the laboratory investigation. Fresh and cured binder characterization tests were carried out on mortar samples meanwhile XRD and thermogravimetric tests were conducted on pastes. For the paste and mortar samples manufacturing, MgO product to GGBS binder proportion chosen was 20 wt% to 80 wt%. For the PC pastes and mortar samples manufacturing, the ratio water to cement was fixed in 1 to 2.5 (w/c = 0.4). For the MgO product samples, the ratio water to binder was fixed in 1 to 1.5 (w/b = 0.6) because of the MgO product mortars workability needs, in accordance with [17-21]. MgO products and GGBS were mixed in a laboratory mortar mixer for 5 min to guarantee the binder homogeneity. For the pastes manufacturing, water was added to the mix of MgO product and GGBS or to PC and mixed for 10 min to guarantee the mix homogeneity and the correct moisture distribution. Paste samples were poured, vibrated and maintained in closed containers till the testing ages of 28 and 90 days. For the mortars manufacturing, MgO products and GGBS were mixed in the same manner described for pastes. Sand was added to the binary binders or to PC and mixed for 5 min. Then water was added and mortars were mixed for 10 min. Fresh mortars were cast into 4x4x16 cm molds and compressed using a vibrating table for 30 s. After compaction, sample surfaces were manually smoothed and maintained in laboratory conditions for 24 h before unmolding. Unmolded mortar samples were cured in water immersion till the testing ages of 7, 14, 21, 28 and 90 days.

Table 1
Chemical composition, fineness and reactivity of the MgO binder constituents and PC.

OXIDES (%)	PC-8	MCB 100	GGBS	PC
MgO	59.67	82.26	9.05	1.21
CaO	9.10	3.79	43.94	70.82
SO_3	6.27	0.21	2.00	4.15
SiO_2	2.80	3.41	32.18	14.12
Fe_2O_3	2.34	2.90	0.33	4.10
Al_2O_3	0.57	0.82	10.40	3.36
Loss of ignition at 1,050 °C	19.25	6.61	0.46	4.97
Reactivity in citric acid (min)	29	2	>600	>600
pH in water	10.66	10.88	9.82	11.88
Free lime (%)	0.81	1.04	0.28	3.67

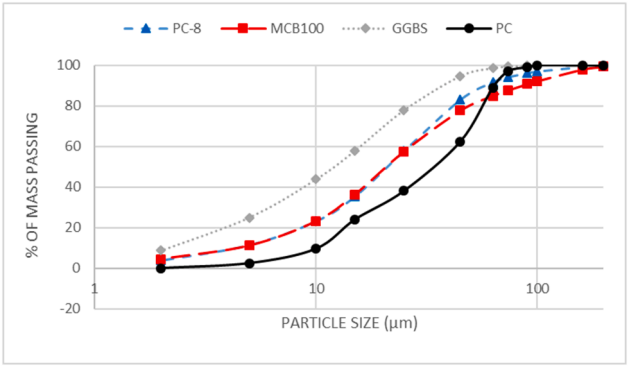

Fig. 2. Granulometric curves of the binder constituents.

2.3. Fresh and cured properties testing methods

The fresh consistency of the mortars were evaluated using the flow table test, in accordance with the standard EN 1015–3. Mortars setting time was determined by means of the Vicat needle method, in accordance with the standard EN 480–2. Samples density was stated as the ratio between the dry mass of each specimen and its corresponding volume, measured by a digital caliper, in accordance with the EN 1015-10. The mechanical properties of the mortars were studied by means of the flexural (FS) and compressive strength (CS) at different curing ages.

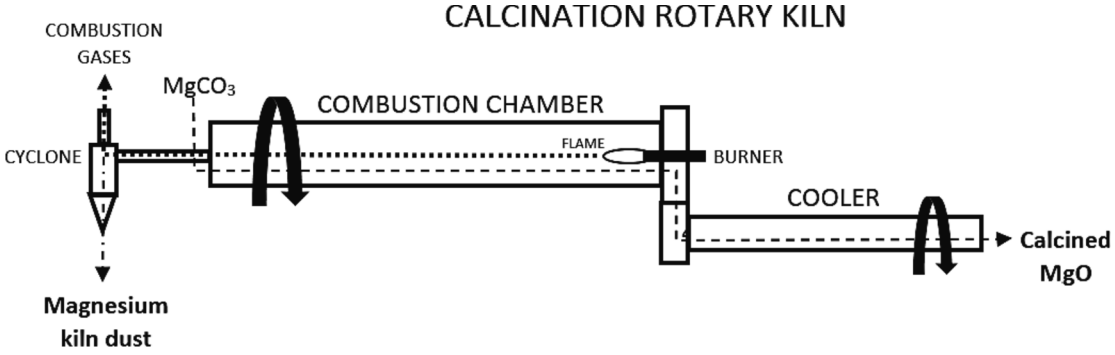

Fig. 1. MgO manufacturing process.

FS and CS tests were carried out in accordance with the standard EN 1015–11.

2.4. Chemical testing methods

At the considered testing ages, samples of each paste combinations were conditioned as follows to completely stop the cementation reactions: 50 g of each paste combination were ground and added to 250 g of isopropanol in a beaker. The mix was shaken with a glass stirrer for 1 min and the result was filtered adding an additional quantity of isopropanol to clean the beaker. Once filtered, the sample was collected and dried for 10 min in an extractor hood and after that the sample was maintained for 24 h at 40 °C in a stove. Once the sample was dried it was maintained in a closed plastic container with silica gel and a CO_2 sorbent till testing.

Specimen pH values were determined following the procedure published in [8]. 10 g of paste specimen samples were dispersed in 100 ml of distilled water. After an hour of mixing, solids were filtered and pH was measured by using a laboratory pH meter with an accuracy of ± 0.01. Crystalline phases and the hydration products present in the paste samples were investigated by XRD testing. This test was performed using a powder diffractometer D8-Advance, Bruker Corp. A Cu-Kα X-ray tube with an input voltage of 40 kV and a current of 40 mA was employed. The samples were scanned for 2 theta value ranging from 4° to 70°, with a step length of 0.05°, scanning rate of 3°/min.

Consumption of MgO, hydration products and M-S-H gels formation were monitored at 28 and 90 days by thermogravimetric analyses (TGA/DTG) in a METTLER-TOLEDO TGA/DSC 3 + system. Tests were conducted with 10 mg of sample under an air flux of 100 ml/min and a heating rate of 10 °C/min from room temperature to 900 °C, with a N_2:O_2 (4:1) oxidizing atmosphere.

3. Results and discussion

3.1. Mortar fresh properties

Table 2 shows the mortar fresh properties.

The fresh consistencies of the mortars observed were 177 mm for the PC combination, 160 mm for the PC-8 + GGBS and 144 mm for the MCB100 + GGBS one. As all the samples were manufactured maintaining constant the aggregates to binder and water to binder ratios, the differences in consistency would be attributed to the binder constituents fineness [22-24]. As expected based on its coarser granulometry, PC mortar showed the lower consistency. Nevertheless the consistent differences observed between the PC-8 + GGBS and the MCB100 + GGBS mortars cannot be attributed only to the small granulometric differences between these two MgO products and would be due to differences of water affinity between PC-8 and MCB100.

The setting time of the considered mortars are provided in Table 2. The initial and final shorter setting times correspond to the PC sample, with 200 and 317 min respectively. PC-8 + GGBS and MCB100 + GGBS mortars showed an increase in initial and final setting times because of their lower pH and rate of pozzolanic reactions compared to PC [22,25].

Table 2
Fresh properties, densities and pH values of the mortars.

Test	Binder		
	PC-8 + GGBS	MCB100 + GGBS	CEM II 32.5
Flow table consistency (mm)	160	144	177
Setting time (minutes)			
Initial	458	478	200
Final	1261	1450	317
Dry density (g/cm^3)	1.88	1.88	1.96
pH			
28 days	11.43	11.47	12.00
90 days	11.49	11.70	12.09

PC-8 + GGBS reached shorter setting times than MCB100 + GGBS, showing its higher hydration ability.

3.2. Mortar cured properties

PC combination reached the highest mortar density, 1.96 g/cm^3, demonstrating the ability of the C-S-H gels to form a denser structure compared to the M-S-H ones [10]. PC-8 + GGBS and MCB100 + GGBS combinations showed no density differences, achieving both mortars 1.88 g/cm^3. The observed lower density of both MgO + GGBS mortars agrees with those obtained by Dave et al. [22] and highlights the direct effect of the binder fineness and the mortar density.

Fig. 3 shows the mortars flexural and compressive strength development up to 90 days.

PC samples showed quick flexural strength development due to its rapid hydration and high reactivity. At 7 days PC mortars reached 4.51 MPa which slowly increased till 5.25 MPa at 90 days. MCB100 + GGBS and PC-8 + GGBS mortars showed a direct flexural strength increase along the curing time. At the age of 7 days MCB100 + GGBS and PC-8 + GGBS mortars reached 1.02 MPa and 2.59 MPa of flexural strength respectively. At the age of 21 days PC-8 + GGBS samples showed a flexural strength of 4.99 MPa, very close to the 5.23 MPa obtained by PC. At the age of 90 days, MCB100 + GGBS and PC-8 + GGBS mortars overcame the PC result, achieving 6.49 MPa and 7.14 MPa, respectively. The lower flexural strength of the MgO-based mortars at the earlier curing ages is probably due to the slower hydration ability and reactivity of these binders, as stated by the setting times test and in accordance with the results obtained by Jin and Altabaa [19] and Bernard et al. [26]. Considering the calcining temperatures, reactivity parameters and fineness of PC-8 and MCB100, the higher flexural strength reached by the PC-8 + GGBS samples compared to these of MBC100 + GGBS is an

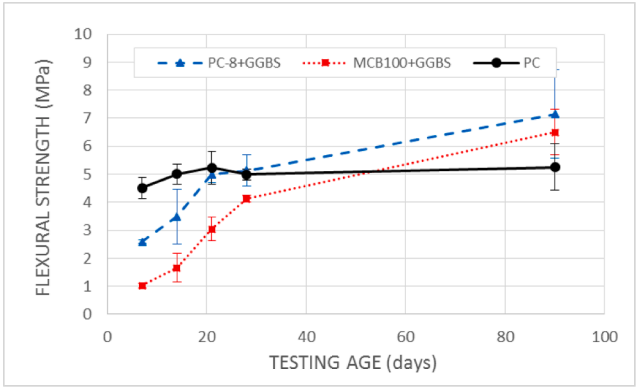

a)

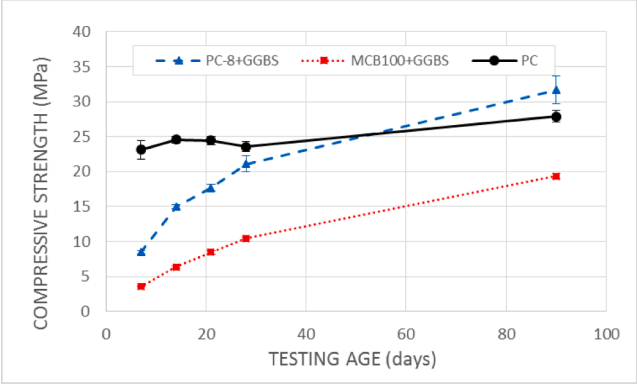

b)

Fig. 3. Mechanical strength of the mortars. a) Flexural strength and b) Compressive strength.

unexpected result. It could be related to the content of CaO of the PC-8 that would hydrate to form C-S-H gels contributing to increase the flexural strength of the PC-8 + GGBS samples [27].

Compressive strengths of mortars are presented in Fig. 3-b. PC samples reached compressive strength of 23.11 MPa at the age of 7 days which increased slightly till 27.90 MPa at 90 days. This compressive strength development agrees with the flexural strength and highlights the quick hydration of the PC compared to the MgO-GGBS binary binders. MCB100 + GGBS and PC-8 + GGBS combinations showed a compressive strength development close to those observed in the flexural strength due to the pozzolanic gels formation [22,28,29]. As well as in the case of the flexural strength, PC-8 + GGBS samples showed higher compressive strength than MCB100 + GGBS at all the curing ages. At 7 days, MCB100 + GGBS mortar showed 3.57 MPa compressive strength, whereas PC-8 + GGBS reached 8.47 MPa. These values increased along the curing time till reaching 19.36 MPa for the MCB100 and 31.68 MPa for the PC-8 at 90 days. Only PC-8 overcame the PC compressive strength between 28 and 90 days.

Flexural and compressive strength test results demonstrated the convenience of the MgO + GGBS binary binders for the manufacturing of ordinary masonry mortars with the required mechanical properties. The higher ability of PC-8, a MKD, was also demonstrated, compared to MCB100, a commercial reactive MgO product, to form cementitious hydraulic gels, that achieved higher mechanical strength than PC.

3.3. Mortar chemical properties

pH values of the considered paste combinations at 28 days and 90 days are shown in Table 2. The pH of the pastes is related to the hydration of MgO and CaO that transform into $Mg(OH)_2$ and $Ca(OH)_2$ respectively, releasing OH^- to the paste dissolution. As expected PC, due to its high content of available CaO, reached pH values of 12.0 at 28 days and 12.08 at 90 days respectively, in accordance with Gu et al. [10] and Shen et al. [6], among others. PC-8 + GGBS paste showed pH values of 11.43 at 28 days and 11.47 at 90 days, while MBC100 + GGBS achieved 11.47 and 11.70 at the same curing ages. These relatively high pH values for MgO-based binders are probably due to the presence of CaO as well in both MgO products as in the GGBS [3,7,8,19]. All the binders showed very close results at both curing ages, probably due to the equilibrium of the precipitation-dissolution of M-S-H and C-S-H gels and $Mg(OH)_2$ and $Ca(OH)_2$ respectively [30].

Fig. 4 shows the XRD diffractograms of the PC, PC-8 + GGBS and MCB100 + GGBS pastes at 28 and 90 days.

MgO, $Mg(OH)_2$, $MgCO_3$ and $CaCO_3$ were identified in the diffractograms of the pastes of PC-8 + GGBS and MCB100 + GGBS based on Jin and al-tabbaa [7], Sonat el al.[8], 2017 and Tran and Scott [31]. MgO in the pastes is related to their peryclase content, due to the calcination of the magnesite rock. Brucite appears as well as in the PC-8 + GGBS as in the MCB100 + GGBS pastes. Its presence demonstrated the existence of reactive MgO in the PC-8 and MCB100 and its ability to hydrate. The intensity of the brucite peaks was higher in the PC-8 + GGBS paste than in the MCB100 + GGBS one, showing a better hydration ability of this combination. For both MgO products, the intensity of the brucite peaks increased since 28 days to 90 days, due to the MgO hydration along the time. The presence of $MgCO_3$ and $CaCO_3$ in the pastes was attributed to non-calcined magnesite and calcite rocks. As expected based on their different degree of calcination, PC-8 containing sample showed a higher content of carbonates than MCB100 ones. M-S-H gels have a low crystallinity structure and they were identified as well as in the PC-8 + GGBS as in the MCB100 + GGBS pastes, as the broad peaks in the 17–28°, 32–39° and 58–62° range 2θ angles [8,32-34].

Fig. 5 shows the TG and first derivative of TG (DTG) results of the binder pastes. Since all samples were thoroughly dried before testing, the loss of mass observed corresponds to the decomposition of hydrate phases [3,8,35]. The first decomposition step generates peaks in the DTG curves centered at about 90–105 °C. These peaks involve the loss of

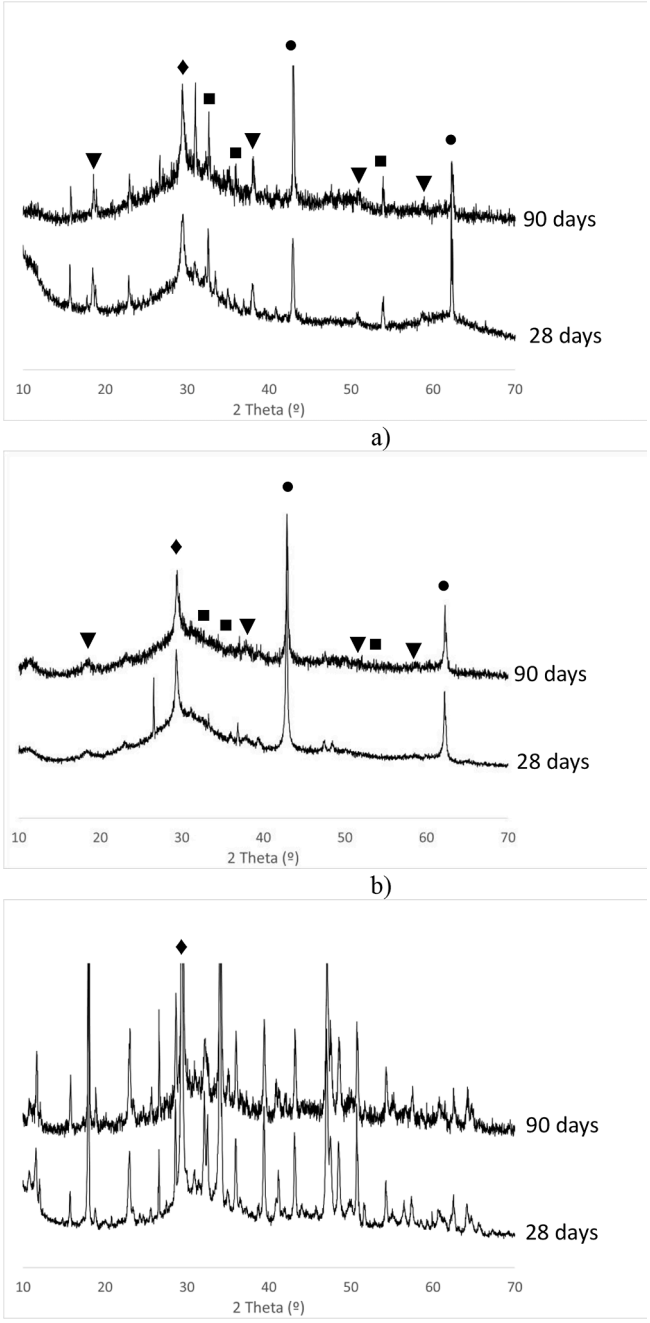

Fig. 4. XRD diffractograms of all paste samples at 28 and 90 days. a) PC-8 + GGBS, b) MCB100 + GGBS and c) PC. (●: MgO, ▼: $Mg(OH)_2$, ■: $MgCO_3$, ◆: $CaCO_3$).

poorly bound water absorbed in the surface and the interlayer of hydration product structures. Cement paste showed the highest loss of mass in this step, demonstrating a higher capacity of C-S-H gels compared to M-S-H ones for the physically bounding of water. PC-8 + GGBS achieved higher loss of mass than MCB100 + GGBS which could be related to the capacity of both binders to produce M-S-H gels, in accordance with the mechanical strength results. PC and MCB100 + GGBS showed a higher loss of mass at 28 days than at 90 days in accordance with the results obtained by Monteagudo et al. [36] but in contradiction with those of Jin and Al-Tabbaa [19]. On the other hand, PC-8 + GGBS reached very close results for both curing ages. This could be due to the different hydration processes and resulting products obtained by each binder because of their different reactivity. The second

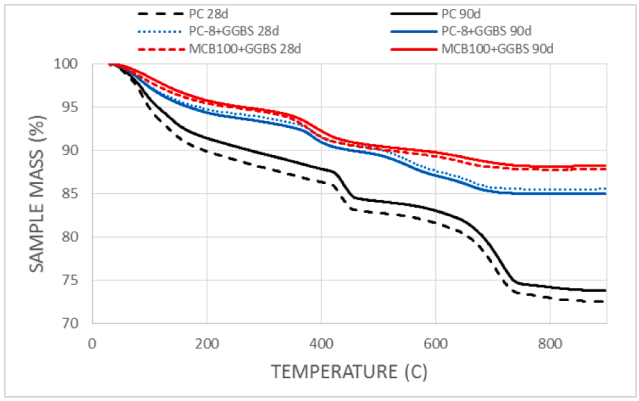

a)

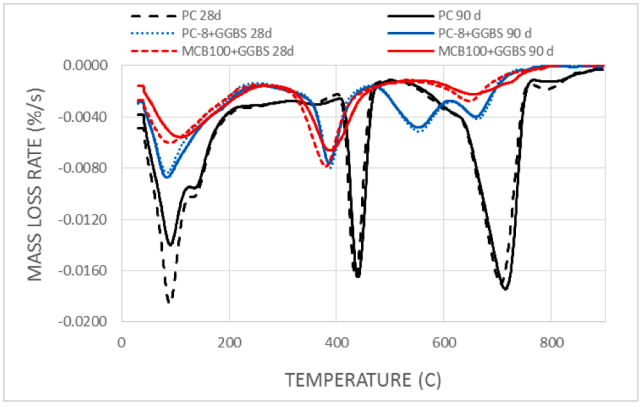

b)

Fig. 5. Thermogravimetric analysis curves for the PC, PC-8 + GGBS and MCB100 + GGBS pastes at 28 and 90 days. a) TG and b) DTG.

decomposition step corresponds to the dehydroxylation of brucite and portlandite [35,37,38]. Thus, brucite decomposition is shown as a peak in the PC-8 + GGBS and MCB100 + GGBS DTG curves at about 390 °C. MCB100 + GGBS showed an expected reduction of this peak because of the brucite consumption from 28 days to 90 days [19]. This reduction was not visible in the PC-8 + GGBS DTG curve that points up the probable consumption of brucite before 28 days in this binder. At 440 °C PC curves show the portlandite dehydroxylation peak [38,39]. In PC-8 + GGBS DTG curves, a peak centered at about 560 °C is observed, corresponding to the M-S-H dehydroxylation or more probably to the magnesite decarbonation [2,7,8,26,40]. Above 650 °C till 750 °C calcite decarbonation occurs [37-39]. PC DTG curve shows a deep decarbonation peak corresponding to the PC limestone content. MCB100 + GGBS and PC-8 + GGBS pastes show in the DTG curves two peaks centered at 655 °C and 665 °C respectively, corresponding to the calcite decomposition [36,40]. The higher loss of ignition at 1,050 °C of the PC-8 compared to MCB100 points out its higher $CaCO_3$ content and would agree with these peaks intensity. Other authors attribute the losses of mass at these temperatures to the dehydroxylation of magnesium or silanol hydroxyl groups [3,8,33,41,42]. The mechanical strength results of the PC-8 + GGBS samples demonstrated the higher ability of this combination to produce M-S-H gels than MCB100 + GGBS one. This also could justify the peaks shown in the DTG curves at 655 °C and 665 °C. So both origins for these peaks are feasible as well as a possible overlapping of dehydroxylation and decarbonation effects [19].

4. Conclusions

In this paper binary binders have been prepared from a commercial and by-product MgO sources, combined with GGBS. The ability of both MgO products for the M-S-H systems formation was evaluated by means of the characterization of fresh mortar properties, mortars mechanical strength and pastes chemical properties. Both MgO binders required higher w/b ratio for workability. PC-8-based binder reached higher consistency than cement but lower than MCB100-based binder. Both MgO-based binders reached identical densities, and slightly lower than PC one, demonstrating the influence of these product fineness and the w/b ratio in the mortar densities. MgO-based binders greatly increase the initial and final setting times compared to PC, related to a lower ability for their hydration and lower reactivity. MgO-based binders showed initial lower mechanical strength that increased along the curing time. Both MgO based mortars overcame PC flexural strength before 90 days, having reached the PC-8 combination the highest flexural strength result. PC-8 containing binder also achieved the highest compressive strength. This demonstrate the good mechanical properties of M-S-H systems compared to the C-S-H at long curing ages ones, and the convenience of PC-8 to produce binary binders with GGBS, compared to MCB100. XRD tests demonstrated the ability of the MgO products to hydrate and to form M-S-H gels. TG/DTG test showed differences in the dehydration, dehydroxilation and decarbonation processes between the M-S-H and the C-S-H systems of the binders considered. The differences observed between the PC-8 + GGBS and MCB100 + GGBS combinations were attributed to the differences of mineralogy and reactivity of both MgO sources. It should be noted that the results and conclusions obtained are applicable to the specific materials used in this investigation and that other MgO products may produce different results. As final conclusion, the higher potential of the MKD as binder component for the mortars manufacturing can be stated, compared to the commercial MgO source. Its longer setting times and higher physical strength are properties with a very wide application range related with large concrete works. Further investigations related with massive concrete structures would be developed, where hydration heat could be more easily dissipated for possible enhancement of the concrete retraction capacity.

Data availability.

The raw data required to reproduce these findings are available from the authors.

CRediT authorship contribution statement

A. Seco: Conceptualization, Methodology, Formal analysis, Writing – original draft, Writing – review & editing, Supervision. **J.M. del Castillo:** Methodology, Formal analysis, Investigation, Writing – review & editing. **S. Espuelas:** Investigation, Writing – review & editing. **S. Marcelino:** Resources, Investigation, Visualization, Project administration. **A.M. Echeverría:** Data curation, Investigation, Funding acquisition.

Declaration of Competing Interest

The authors declare that they have no known competing financial interests or personal relationships that could have appeared to influence the work reported in this paper.

Acknowledgements

This work was funded by Gobierno de Navarra and Fondo Europeo de Desarrollo Regional (FEDER) by the *estudio y aplicación de coproductos basados en el óxido de magnesio como estabilizadores de suelos con contenido en sulfatos* (Reference: 0011-1365-2018-000093), research project.

References

[1] Y. Li, J. Sun, B. Chen, Experimental study of magnesia and M/P ratio influencing properties of magnesium phosphate cement, Constr. Build. Mater. 65 (2014) 177–183, https://doi.org/10.1016/j.conbuildmat.2014.04.136.

[2] C. Roosz, S. Grangeon, P. Blanc, V. Montouillout, B. Lothenbach, P. Henocq, E. Giffaut, P. Vieillard, S. Gaboreau, Crystal structure of magnesium silicate hydrates (M-S-H): The relation with 2:1 Mg-Si phyllosilicates, Cem. Concr. Res. 73 (2015) 228–237, https://doi.org/10.1016/j.cemconres.2015.03.014.

[3] E. Bernard, B. Lothenbach, C. Chlique, M. Wyrzykowski, A. Dauzères, I. Pochard, C. Cau-Dit-Coumes, Characterization of magnesium silicate hydrate (M-S-H), Cem. Concr. Res. 116 (2019) 309–330, https://doi.org/10.1016/j.cemconres.2018.09.007.

[4] C. Unluer, in: Carbon dioxide sequestration in magnesium-based binders, Elsevier Ltd, 2018, https://doi.org/10.1016/b978-0-08-102444-7.00007-1.

[5] Y. Yi, X. Zheng, S. Liu, A. Al-Tabbaa, Comparison of reactive magnesia- and carbide slag-activated ground granulated blastfurnace slag and Portland cement for stabilisation of a natural soil, Appl. Clay Sci. 111 (2015) 21–26, https://doi.org/10.1016/j.clay.2015.03.023.

[6] W. Shen, L. Cao, Q. Li, Z. Wen, J. Wang, Y. Liu, R. Dong, Y. Tan, R. Chen, Is magnesia cement low carbon? Life cycle carbon footprint comparing with Portland cement, J. Clean. Prod. 131 (2016) 20–27, https://doi.org/10.1016/j.jclepro.2016.05.082.

[7] F. Jin, A. Al-Tabbaa, Thermogravimetric study on the hydration of reactive magnesia and silica mixture at room temperature, Thermochim Acta 566 (2013) 162–168, https://doi.org/10.1016/j.tca.2013.05.036.

[8] C. Sonat, N.T. Dung, C. Unluer, Performance and microstructural development of MgO–SiO2 binders under different curing conditions, Constr. Build. Mater. 154 (2017) 945–955, https://doi.org/10.1016/j.conbuildmat.2017.08.020.

[9] F. Cao, P. Yan, The influence of the hydration procedure of MgO expansive agent on the expansive behavior of shrinkage-compensating mortar, Constr. Build. Mater. 202 (2019) 162–168, https://doi.org/10.1016/j.conbuildmat.2019.01.016.

[10] K. Gu, F. Jin, A. Al-Tabbaa, B. Shi, C. Liu, L. Gao, Incorporation of reactive magnesia and quicklime in sustainable binders for soil stabilisation, Eng. Geol. 195 (2015) 53–62, https://doi.org/10.1016/j.enggeo.2015.05.025.

[11] A. Seco, F. Ramírez, L. Miqueleiz, B. Garci, E. Prieto, The use of non-conventional additives in Marls stabilization, Appl. Clay Sci. 51 (2011) 419–423, https://doi.org/10.1016/j.clay.2010.12.032.

[12] A. Seco, F. Ramírez, L. Miqueleiz, B. García, Stabilization of expansive soils for use in construction, Appl. Clay Sci. 51 (2011) 348–352, https://doi.org/10.1016/j.clay.2010.12.027.

[13] A. Seco, L. Miqueleiz, E. Prieto, S. Marcelino, B. García, P. Urmeneta, Sulfate soils stabilization with magnesium-based binders, Appl. Clay Sci. 135 (2017) 457–464, https://doi.org/10.1016/j.clay.2016.10.033.

[14] S. Espuelas, J. Omer, S. Marcelino, A.M. Echeverría, A. Seco, Magnesium oxide as alternative binder for unfired clay bricks manufacturing, Appl. Clay Sci. 146 (2017) 23–26.

[15] A. Seco, P. Urmeneta, E. Prieto, S. Marcelino, B. García, L. Miqueleiz, Estimated and real durability of unfired clay bricks: Determining factors and representativeness of the laboratory tests, Constr. Build. Mater. 131 (2017) 600–605, https://doi.org/10.1016/j.conbuildmat.2016.11.107.

[16] M. Pisciotta, H. Pilorgé, J. Feldmann, R. Jacobson, J. Davids, S. Swett, Z. Sasso, J. Wilcox, Current state of industrial heating and opportunities for decarbonization, Prog. Energy Combust. Sci. (2022). https://doi.org/10.1016/j.pecs.2021.100982.

[17] L.J. Vandeperre, M. Liska, A. Al-Tabbaa, Microstructures of reactive magnesia cement blends, Cem. Concr. Compos. 30 (2008) 706–714, https://doi.org/10.1016/j.cemconcomp.2008.05.002.

[18] M. Liska, A. Al-Tabbaa, Performance of magnesia cements in pressed masonry units with natural aggregates: Production parameters optimisation, Constr. Build. Mater. 22 (2008) 1789–1797, https://doi.org/10.1016/j.conbuildmat.2007.05.007.

[19] F. Jin, A. Al-Tabbaa, Strength and hydration products of reactive MgO-silica pastes, Cem. Concr. Compos. 52 (2014) 27–33, https://doi.org/10.1016/j.cemconcomp.2014.04.003.

[20] A. Kalagri, I. Karatasios, V. Kilikoglou, The effect of aggregate size and type of binder on microstructure and mechanical properties of NHL mortars, Constr. Build. Mater. 53 (2014) 467–474, https://doi.org/10.1016/j.conbuildmat.2013.11.111.

[21] S. Cunha, J.B. Aguiar, A. Tadeu, Thermal performance and cost analysis of mortars made with PCM and different binders, Constr. Build. Mater. 122 (2016) 637–648, https://doi.org/10.1016/j.conbuildmat.2016.06.114.

[22] N. Dave, A.K. Misra, A. Srivastava, S.K. Kaushik, Experimental analysis of strength and durability properties of quaternary cement binder and mortar, Constr. Build. Mater. 107 (2016) 117–124, https://doi.org/10.1016/j.conbuildmat.2015.12.195.

[23] S. Espuelas, A.M. Echeverria, S. Marcelino, E. Prieto, A. Seco, Technical and environmental characterization of hydraulic and alkaline binders, J. Clean. Prod. 196 (2018) 1306–1313, https://doi.org/10.1016/j.jclepro.2018.06.090.

[24] C. Giordani, A.B. Masuero, Blended mortars: Influence of the constituents and proportioning in the fresh state, Constr. Build. Mater. 210 (2019) 574–587, https://doi.org/10.1016/j.conbuildmat.2019.02.077.

[25] L. Mo, M. Liu, A. Al-Tabbaa, M. Deng, W.Y. Lau, Deformation and mechanical properties of quaternary blended cements containing ground granulated blast furnace slag, fly ash and magnesia, Cem. Concr. Res. 71 (2015) 7–13, https://doi.org/10.1016/j.cemconres.2015.01.018.

[26] E. Bernard, B. Lothenbach, D. Rentsch, I. Pochard, A. Dauzères, Formation of magnesium silicate hydrates (M-S-H), Phys. Chem. Earth. 99 (2017) 142–157, https://doi.org/10.1016/j.pce.2017.02.005.

[27] T. Zhang, C.R. Cheeseman, L.J. Vandeperre, Development of low pH cement systems forming magnesium silicate hydrate (M-S-H), Cem. Concr. Res. 41 (2011) 439–442, https://doi.org/10.1016/j.cemconres.2011.01.016.

[28] C. Namarak, P. Satching, W. Tangchirapat, C. Jaturapitakkul, Improving the compressive strength of mortar from a binder of fly ash-calcium carbide residue, Constr. Build. Mater. 147 (2017) 713–719, https://doi.org/10.1016/j.conbuildmat.2017.04.167.

[29] T.P. Huynh, D.H. Vo, C.L. Hwang, Engineering and durability properties of eco-friendly mortar using cement-free SRF binder, Constr. Build. Mater. 160 (2018) 145–155, https://doi.org/10.1016/j.conbuildmat.2017.11.040.

[30] Z. Li, T. Zhang, J. Hu, Y. Tang, Y. Niu, J. Wei, Q. Yu, Characterization of reaction products and reaction process of MgO-SiO 2–H2O system at room temperature, Constr. Build. Mater. 61 (2014) 252–259, https://doi.org/10.1016/j.conbuildmat.2014.03.004.

[31] H.M. Tran, A. Scott, Strength and workability of magnesium silicate hydrate binder systems, Constr. Build. Mater. 131 (2017) 526–535, https://doi.org/10.1016/j.conbuildmat.2016.11.109.

[32] D.R.M. Brew, F.P. Glasser, Synthesis and characterisation of magnesium silicate hydrate gels, Cem. Concr. Res. 35 (2005) 85–98, https://doi.org/10.1016/j.cemconres.2004.06.022.

[33] E. Bernard, B. Lothenbach, C. Cau-Dit-Coumes, C. Chlique, A. Dauzères, I. Pochard, Magnesium and calcium silicate hydrates, Part I: Investigation of the possible magnesium incorporation in calcium silicate hydrate (C-S-H) and of the calcium in magnesium silicate hydrate (M-S-H), Appl. Geochem. 89 (2018) 229–242, https://doi.org/10.1016/j.apgeochem.2017.12.005.

[34] J. Zheng, X. Sun, L. Guo, S. Zhang, J. Chen, Strength and hydration products of cemented paste backfill from sulphide-rich tailings using reactive MgO-activated slag as a binder, Constr. Build. Mater. 203 (2019) 111–119, https://doi.org/10.1016/j.conbuildmat.2019.01.047.

[35] D. Zhang, X. Cai, B. Jaworska, Effect of pre-carbonation hydration on long-term hydration of carbonation-cured cement-based materials, Constr. Build. Mater. 231 (2020), 117122, https://doi.org/10.1016/j.conbuildmat.2019.117122.

[36] S.M. Monteagudo, A. Moragues, J.C. Gálvez, M.J. Casati, E. Reyes, The degree of hydration assessment of blended cement pastes by differential thermal and thermogravimetric analysis. Morphological evolution of the solid phases, Thermochim Acta 592 (2014) 37–51, https://doi.org/10.1016/j.tca.2014.08.008.

[37] W. Deboucha, N. Leklou, A. Khelidj, M.N. Oudjit, Hydration development of mineral additives blended cement using thermogravimetric analysis (TGA): Methodology of calculating the degree of hydration, Constr. Build. Mater. 146 (2017) 687–701, https://doi.org/10.1016/j.conbuildmat.2017.04.132.

[38] P. Czapik, J. Zapała-Sławeta, Z. Owsiak, P. Stępień, Hydration of cement by-pass dust, Constr. Build. Mater. 231 (2020) 117139.

[39] B.L. de Sena Costa, J.C. de Oliveira Freitas, P.H. Silva Santos, R. Gomes da Silva Araújo, J.F. dos Santos Oliveira, D.M. de Araújo Melo, Study of carbonation in a class G Portland cement matrix at supercritical and saturated environments, Constr. Build. Mater. 180 (2018) 308–319.

[40] Y. Zhang, Y. Sun, K. Xu, Z. Yuan, J. Zhang, R. Chen, H. Xie, R. Cheng, Brucite modified epoxy mortar binders: Flame retardancy, thermal and mechanical characterization, Constr. Build. Mater. 93 (2015) 1089–1096, https://doi.org/10.1016/j.conbuildmat.2015.05.037.

[41] E. Bernard, B. Lothenbach, F. Le Goff, I. Pochard, A. Dauzères, Effect of magnesium on calcium silicate hydrate (C-S-H), Cem. Concr. Res. 97 (2017) 61–72, https://doi.org/10.1016/j.cemconres.2017.03.012.

[42] E. Bernard, A. Dauzères, B. Lothenbach, Magnesium and calcium silicate hydrates, Part II: Mg-exchange at the interface "low-pH" cement and magnesium environment studied in a C-S-H and M-S-H model system, Appl. Geochemistry. 89 (2018) 210–218, https://doi.org/10.1016/j.apgeochem.2017.12.006.